Computational Modeling of Temperature Elevation and Thermoregulatory Response in the Brains of Anesthetized Rats Locally Exposed at 1.5 GHz

Akimasa Hirata[1], Hiroshi Masuda[2], Yuya Kanai[1], Ryuichi Asai[1], Osamu Fujiwara[1], Takuji Arima[3], Hiroki Kawai[3], Soichi Watanabe[3], Isabelle Lagroye[2], and Bernard Veyret[2]

[1]: Dept. of Computer Science and Engineering, Nagoya Institute of Technology, Nagoya 466-8555, Japan.
[2]: University of Bordeaux, IMS lab., Pessac 33607, France.
[3]: EMC Group, National Institute of Information and Communications Technology, Tokyo 184-8795, Japan

Abstract

The dominant effect of human exposures to microwaves is caused by temperature elevation (“thermal effect”). In the safety guidelines/standards, the specific absorption rate (SAR) averaged over a specific volume is used as a metric for human protection from localized exposure. Further investigation on the use of this metric is required, especially in terms of thermophysiology. The World Health Organization (2006) has given high priority to research into the extent and consequences of microwave-induced temperature elevation in children. In the present study, an electromagnetic-thermal computational code was developed to model electromagnetic power absorption and resulting temperature elevation leading to changes in active blood flow in response to localized 1.457-GHz exposure in rat heads. Both juvenile (4-week-old) and young adult (8-week-old) rats were considered. The computational code was validated against measurements for 4- and 8-week-old rats. Our computational results suggest that blood flow rate depends on both brain and core temperature elevations. No significant difference was observed between thermophysiological responses in 4- and 8-week-old rats under these exposure conditions. The computational model developed herein is thus applicable to set exposure conditions for rats in laboratory investigations, as well as in planning treatment protocols in the thermal therapy.

Keyword: localized exposure, radio-frequency dosimetry, electromagnetic heating, thermophysiological response

1. Introduction

There has been increasing public concern about potential adverse health effects of exposure to electromagnetic fields. In the radiofrequency and microwave (MW) ranges, temperature elevation (1-2°C) resulting from energy absorption is known to be the dominant mechanism inducing adverse health effects such as heat exhaustion and heat stroke (ACGIH 1996). This threshold temperature elevation is used as a basis for international safety standards/guidelines (ICNIRP 1998, IEEE 2005). In these standards/guidelines, the 10 g averaged specific absorption rate (SAR) and whole-body SAR are used as metrics for human protection from localized and whole-body exposures, respectively, to prevent excess temperature elevation. For occupational exposure limits of local and whole-body average SARs are 10 W/kg and 0.4 W/kg, respectively, while a reduction factor of 5 is applied for the general public.

The whole-body SAR limits are mainly based on small animal experiments carried out in the 1980s. According to ICNIRP (1998), laboratory animals exposed to MW at and above 4 W/kg exhibited a characteristic pattern of thermoregulatory behavior (Michaelson 1983). In addition, at SAR values in the 1–3 W/kg range, rats and monkeys showed decreased task performance (Stern 1979, Adair and Adams 1980, D'Andrea et al 1986). The rationale for the IEEE standard (2005) is based on behavioral effects (work stoppage) in rodents and non-human primates exposed for about 1 hour at the 4 W/kg SAR threshold associated with temperature elevation (D'Andrea et al 2003). The relationship between whole-body SAR and core temperature elevation has been investigated in humans (Foster and Adair 2004, Hirata et al 2008) and animals (Hirata et al 2010).

The local SAR limit was determined to prevent thermal ocular damage (ICNIRP 1998). Temperature elevation from localized MW exposure was investigated via modeling in humans and animals, and summarized in (ICNIRP 2009). However, little information is available concerning the biological effects of local MW exposure, especially on the brain. Only a few research groups have reported adverse health effects in rodents below the exposure limit (Alto et al 2006, Huber et al 2005, Salford et al 2003) and other studies have failed to confirm their findings (de Gannes et al 2009, Kuribayashi et al 2005, Masuda et al 2009, McQuade et al 2009, Mizuno et al 2009, Tsurita et al 2000).

The rationale for the use of SAR as a metric for local exposure has been challenged, especially with respect to local and systemic physiological responses, including changes in blood flow (Masuda et al 2007). We recently measured local blood flow in rat brains locally exposed to MW above 6.14 W/kg (brain averaged SAR: BASAR) and found a dose-dependent elevation in blood flow (Masuda et al 2011). Moreover, the correlation between temperature elevation and blood flow was observed in both cortex and rectum during exposure. Although these findings strongly suggest a temperature-dependent variation in blood flow under local

exposure conditions, further studies are required to clarify this relationship. Thus, a physical approach using computational modeling is a good strategy, in view of the technical difficulties of in vivo studies, such as side effects of anesthesia (Adair et al 2004, Hirata et al 2006b) and interference with bioinstruments subjected to high-level MW exposure.

The 2006 RF research agenda of the World Health Organization gave high priority to research aimed at improving dosimetric models of RF deposition in animals and humans, combined with appropriate thermoregulatory models. No computational modeling besides our own (Hirata et al 2006, 2010) has succeeded in investigating both local and core temperatures simultaneously in an anatomically based model, in spite of the fact there is a need to determine the threshold inducing the thermophysiological response to local MW exposure and the age-dependence of that threshold.

The purpose of the present study was therefore to develop a computational model to simulate variations in temperature and blood flow rate in the rat brain under intense local MW exposure, and to compare the thermal model in young adult rats (8-week-old) with that of juvenile (4-week-old) ones. The key point in this model is that it considered the dependence of blood flow rate on local and core temperatures. First, we modeled the temperature dependence of blood flow rate in the brain. The computed temperature elevation in rats was then compared with measurements to validate our computational models.

2. Model and methods

2.1. Animal Experiment

Animal preparation An animal experiment was conducted to measure physiological parameters and to validate our computational model. The 4- and 8-week-old male Sprague-Dawley rats (n=18 for each age) used in the experiment were cared for and handled in accordance with the ethical guidelines for animal experiments at the National Institute of Public Health, Japan. The average weights of the 4- and 8-week-old rats were 103 g ±6% and 295 g ±8%, respectively. The rats were anesthetized using an intramuscular injection of ketamine (100 mg/kg) and xylazine (10 mg/kg), together with a subcutaneous injection of pentobarbital (12.5 mg/kg) and immobilized in an acrylic stereotaxic apparatus designed for this experiment (see Fig. 1). Since anesthesia is known to reduce blood flow and basal metabolic rate and inactivate or attenuate the thermoregulatory response (Adair and Black 2003, Hirata et al 2006), a warm water-heated pad was inserted underneath the rat to compensate for the reduction in basal metabolism. Water and room temperatures were kept at ca. 42°C (see Appendix) and 23°C, respectively.

Measurement of physiological parameters Two physiological parameters, local cerebral

blood flow and temperature in two regions (parietal cortex and rectum) were simultaneously measured using a Doppler blood flow meter (FLO-C1, OMEGAWAVE, Inc., Tokyo, Japan) and an optical fiber thermometer (m600, Luxtron Corp., USA). The right parietal skin was locally excised and the skull of the right hemisphere exposed. Three independent holes (0.5 mm in diameter and 1.0 mm apart) were drilled into the skull just above the parietal cortex. The holes were located 3-4 mm posterior to the bregma and 3-4 mm right of the midline. Two optical fibers (0.2 mm in diameter), connected to the Doppler blood flow meter, and one optical probe (0.5 mm in diameter), connected to the thermometer, were inserted independently through the holes and placed on the dura mater above the parietal cortex. The other thermometer probe was inserted into the rectum. These probes were all made of non-metallic material. The accuracy and resolution of the thermometer were 0.1°C and 0.01°C, respectively. The blood flow and temperature signals were recorded via an A/D converter using a 1.0 Hz sampling rate.

MW exposure The animals' heads were locally exposed to 1,457 MHz MW, which are used for wireless communications in Japan, emitted by a figure-8 loop antenna (Arima et al 2011). The target area is located underneath the antenna (its diameter is 7.5 mm and thickness 0.5 mm). The ratio of the target-area SAR to the whole-body average SAR is greater than 30 in the four-week rat model. Each rat was placed in the manipulator system fitted with the antenna, positioned 4 mm above the parietal bone. Exposure duration was six minutes. The BASARs, quantified using the numerical rat models (described below), were 167, 57, and 17 W/kg for 4-week-old rats (n=6 in each intensity) and 300, 150, and 75 W/kg for 8-week-old rats (n=6 in each intensity). Two physiological parameters, temperature and cerebral blood flow, were measured simultaneously during exposure. These exposure levels were calculated using the 4- and 8-week-old rat models. The exposure levels were defined in terms of BASAR, since the distance between antenna and rat was different for different-aged models. Maximum output power were calculated from our analytical results (Hirata et al 2009a) to induce a maximum core temperature elevation of 2°C at the end of the six-minute exposure.

2.2. Numerical rat model

Numerical models including the exposure system were developed on the basis of X-ray CT images (Figure 1). The resolution of the models was 0.5 mm. The rat model at ages 4 and 8 weeks consisted of six tissues (skin, muscle, fat, bone, brain, and eye). The length, weight, and brain weight used in the rat models were 142 mm, 89 g, and 1.7 g, respectively, for the 4-week-old and 212 mm, 265 g, and 1.9 g, respectively, for the 8-week-old.

2.3. SAR computation

The FDTD method (Taflove and Hagness 1995) was first used to quantify the MW power absorbed in the rat phantom. Perfectly-matched layers were used as the absorbing boundary to truncate the computational region. The cell size of the FDTD domain was 0.5 mm, which coincided with the tissue model resolution. The difference in dielectric properties of tissues between 4- and 8-week-old rats are less than 10% (Peyman et al 2001, Peyman 2011) and the same parameters were thus used for 4- and 8-week-old rats. The dielectric properties of the tissues were taken from the data of 4-week-old rats in Peyman et al (2001). The dielectric properties of the fat and eye, however, were not measured in that study and thus chosen as the values of average fat and average eye in Gabriel (1996). Note that small changes in the dielectric properties do not affect the SAR and temperature elevation significantly (Fujimoto et al 2006, Christ et al 2010).

Our computation considered the harmonically varying fields. SAR is defined as

$$SAR = \frac{\sigma}{2\rho} |\hat{E}|^2 = \frac{\sigma}{2\rho}(|\hat{E}_x|^2 + |\hat{E}_y|^2 + |\hat{E}_z|^2) \quad (1)$$

where $\hat{E}_x$, $\hat{E}_y$, and $\hat{E}_z$ are the peak values of the electric field components and σ and ρ denote the conductivity and mass density of the tissue, respectively. In the following discussion, BASAR is used as an index.

2.4. Temperature computation

In the present study, we considered an active blood flow model in anesthetized rats. The formula for temperature calculation in a rabbit model was presented in our previous study (Hirata et al 2006, 2010). Rabbits are rodents animal with virtually nonfunctional sweat glands (Marai et al 2002), allowing us to neglect the heat control mechanism via sweat. In view of this feature, we applied a human active blood flow model to rabbit skin and inner tissue. Rats are also rodents that have no sweat glands, so it was appropriate to use the rabbit active blood flow model. In addition, a new model simulating rat cerebral blood flow was developed and combined with the existing model.

Bioheat equation The bioheat equation (Pennes 1948) was used to calculate the temperature elevation in the rat model:

$$C(\boldsymbol{r})\rho(\boldsymbol{r})\frac{\partial T(\boldsymbol{r},t)}{\partial t} = \nabla\cdot(K(\boldsymbol{r})\nabla T(\boldsymbol{r},t)) + \rho(\boldsymbol{r})SAR(\boldsymbol{r}) + A(\boldsymbol{r}) - B(\boldsymbol{r},t)(T(\boldsymbol{r},t) - T_B(t)) \quad (2)$$

where $T(\mathrm{r},t)$ and $T_B(t)$ are the tissue and blood temperatures, respectively. *C* is the specific heat and *K* the thermal conductivity of tissue, *A* the basal metabolism per unit volume, and *B* the

term associated with blood flow. The boundary condition between ambient air and tissue for (2) is given by the following equation:

$$-K(r)\frac{\partial T(\boldsymbol{r},t)}{\partial n} = h\cdot(T_s(\boldsymbol{r},t) - T_e(t)) \quad (3)$$

where h, T_s, and T_e denote the heat transfer coefficient, surface temperature, and air temperature, respectively. The heat transfer coefficient h is given by the summation of radiative, convective, and evaporative heat loss.

In order to satisfy the thermodynamic laws, blood temperature varied according to the following equation (Bernardi et al 2003, Hirata et al 2009b):

$$T_B(t) = T_{B0} + \int_t \frac{Q_{BT}(t)}{C_B\rho_B V_B}dt \quad (4)$$

$$Q_{BT}(t) = \int_V B(t)(T_B(t) - T(\boldsymbol{r},t))dV \quad (5)$$

where Q_{BT} is the rate of heat transfer from tissues to blood. C_B (4000 J/kg °C), ρ_B (1050 kg/m3), and V_B denote the specific heat, mass density, and total volume of blood, respectively. Blood temperature was assumed to be constant over the whole body in rats, in view of the fact that the blood circulates throughout the human body in one minute or less (Follow and Neil 1971). The average blood volume per unit of rat body mass was 64 ml/kg (Lee and Blaufox 1985). The blood volume was thus set at 5.6 ml and 17.2 ml for the 4- and 8-week-old rats, respectively. It should be noted that Q_{Bnet} in equation (6) was substituted for Q_{BT} in equation (4) to evaluate the net heat transfer rate from body tissues to blood as follows:

$$Q_{Bnet}(t) = Q_{BT}(t) - Q_{BT}(0). \quad (6)$$

It should also be noted that equation (6) is essential, as the result of equation (4) is not zero even at time t = 0, due to some computational simplifications or assumptions, including a discretized anatomically-based model with finite resolution, uniform distribution of blood temperature over the body, and uncertainty in the basal metabolism rate of tissues depending on individual and body parts (Hirata and Fujiwara 2009).

Thermoregulatory response Blood flow regulation, modulated by tissue temperature, was modeled as a thermoregulatory response. To consider the tissue-dependence of this thermoregulatory response, three regulation models were developed, for skin, brain, and other tissues, and introduced into equations (2) and (5).

Skin blood flow is known to be modulated by hypothalamus temperature as well as local skin temperature. Blood flow regulation in the skin is expressed in terms of temperature elevation in the hypothalamus $T_H - T_{H0}$ and average temperature elevation in the skin ΔT_S :

$$B(\mathbf{r},T(\mathbf{r},t)) = (B_0(\mathbf{r}) + F_{HB}(T_H(t) - T_{H0}) + F_{SB}\Delta T_S(t)) \cdot 2^{(T(\mathbf{r},t)-T_0(\mathbf{r}))/6} \quad (7)$$

$$\Delta T_S(t) = \int_S (T(\mathbf{r},t) - T_0(\mathbf{r}))dS / S. \quad (8)$$

where T_0 is the temperature under steady-state without heat load. F_{HB} and F_{SB} are the weighting coefficients, characterizing the feedback signal between blood flow and temperatures in the hypothalamus and skin, respectively. The previous study reported that F_{HB} and F_{SB} were 17500 W/(m^3 ^{o}C) and 1100 W/(m^3 ^{o}C), respectively (Bernardi et al 2003). In a pilot study using 4- and 8-week-old rats, local brain exposure of MW did not elevate blood flow in the foot skin, up to temperature elevations of 1.5^{o}C in the foot skin at maximal BASAR (data not shown). Thus, the blood flow in the skin is assumed to be constant in the model over the body during exposure.

Blood flow regulation in the brain was considered in a different manner, based on measured blood flow rates in the animal experiment using rats. Specifically, the blood flow rate in the brain was expressed by the following equation, analogous to equation (7), i.e., the blood flow rate was assumed to depend on rectum and brain temperature elevations.

$$B(\mathbf{r},T(\mathbf{r},t)) = (B_0(\mathbf{r}) + F_{RB}(T_B(t) - T_B(0)) \cdot 2^{(T(\mathbf{r},t)-T_0(\mathbf{r}))/F_{BB}} \quad (9)$$

where F_{RB} and F_{BB} are the weighting coefficients, characterizing the feedback signal between blood flow and rectum and brain temperature, respectively.

The regulation of blood flow in tissues other than skin and brain was simplified and governed by the local tissue temperature. When the temperature remained below a certain level, blood flow was equal to its basal value B_0. Once the local temperature exceeded the threshold, blood flow elevated almost linearly with temperature in order to eliminate excess heat. Temperature regulation in humans is expressed by the following equations (Hoque and Gandhi 1988):

$$B(\mathbf{r},T(\mathbf{r},t)) = B_0(\mathbf{r}), \qquad T(\mathbf{r},t) \le T_0(\mathbf{r}) \quad (10)$$

$$B(\mathbf{r},T(\mathbf{r},t)) = B_0(\mathbf{r})\left(1 + (\alpha - 1)\frac{T(\mathbf{r},t) - T_0(\mathbf{r})}{\Delta T}\right), \qquad T_0(\mathbf{r}) < T(\mathbf{r},t) < T_0(\mathbf{r}) + \Delta T \quad (11)$$

$$B(\mathbf{r},T(\mathbf{r},t)) = \alpha B_0(\mathbf{r}), \qquad T(\mathbf{r},t) > T_0(\mathbf{r}) + \Delta T \quad (12)$$

where ΔT denotes the threshold temperature elevation at which the blood flow saturates. Equations (10)-(12) were slightly modified from the original equations given by Hoque and Gandhi (1988). The threshold temperature at which the blood flow is activated was chosen as the set temperature, instead of the constant temperature of 39°C. This is because temperature elevation is more essential than absolute temperature in inducing the thermoregulatory response (Hirata et al 2010). The coefficient α must be larger than 1. The uncertainty in T_{act}, T_{sat} and α may not affect computed brain and rectal temperatures, which are of interest in the present study.

This is because the computed brain temperature is dominantly affected by the blood flow in the brain, which has been modeled by (9) using measured blood flow. In addition, rectal temperature is well estimated based on the heat balance of the body (Hirata et al 2009a). In this study, this effect was neglected based on the parametric study given in Appendix B, even though the blood flow in the inner tissue except for the brain was not measured.

In our blood flow regulation models, temperature elevations in the hypothalamus and rectum were assumed to be identical to those in the blood, in view of the high blood flow rates in these regions.

2.5. Thermal constants

Table 1 lists thermal constants of tissues, which were adapted to our rat model. The specific heat and thermal conductivity of tissues were extrapolated on the basis of tissue water content (Cooper and Trezek 1971, ICRP 1975). Blood perfusion removes the heat developed and carries it over to the surrounding tissues. The effective thermal conductivity was proposed to compensate for that effect (Creeze et al 1990). However, that effect was considered in part in Eqs. (4) and (5), in addition that the blood circulates throughout the rats in a time shorter than one minute, which is that for the human body (Follow and Neil 1971). Thus, the thermal conductivities shown in Cooper and Trezek (1971) are used. The basal metabolic rate was estimated by assuming that it was proportional to blood flow (Gordon et al 1976). The terms associated with blood flow for tissues except the brain were extrapolated from the data for different animals, considering the correlation between body mass and basal metabolic rate (Tuma et al 1985). The term associated with brain blood flow was derived from our measured data. The maximum difference between 4- and 8-week-old rats was 10%. We used the following heat transfer coefficients: 0.5 $W/m^2/^oC$ between skin and air/heating pad and 8.1 $W/m^2/^oC$ between inner air and lung as in Hirata *et al* (2010). The basal metabolism and heat transfer from the rat body to the air were balanced using these thermal parameters.

2.6. Definition of the brain region studied in the rat model

Temperature elevations and blood flow variations were evaluated in a defined brain region of the rat model. A rectangular area (12 mm x 6.1 mm for 4-week-old, 12 mm x 7.2 mm for 8-week-old) within the brain surface was chosen as the defined region (Figure 2). The reference point at the center of the rectangular area was positioned just under the center of the 8-shaped loop antenna.

3. Results

3.1. Derivation of parameters associated with the blood flow rate in the brain

It was necessary to determine the F_{RB} and F_{BB} parameters in equation (9) to compute the temperature elevations in the brain, allowing for the thermoregulation. The parameters were estimated using a least-squares regression between the time course of cerebral blood flow and the temperatures in the rectum and brain during 6-min MW exposure. F_{RB} and F_{BB} were equal to 0.054 and 19, respectively in 4-week-old rats (n=6) at 167 W/kg, and 0.050 and 31, respectively in 8-week-old rats (n=6) at 300 W/kg.

3.2. Computation of the SAR and temperature distributions in the numerical rat model

Figures 3(a) and 4(a) illustrate the SAR distribution under MW exposure in the 4- and 8-week-old rat models, respectively. The maximum SAR in both models was calculated to be around the top of the head, corresponding to the position immediately underneath the figure-8 loop antenna. BASARs in the 4- and 8-week-old models were 11 and 19 times larger than the whole-body average SARs (WBSAR), respectively. These results suggest that MW power was mainly absorbed around the top of the head. In addition, the inter-age difference in the BASAR/WBSAR ratios seemed to be directly linked to body dimensions.

Figures 3(b) and 4(b) show the distribution of temperature elevations after 6-min exposure in the 4- and 8-week-old models, respectively. The distribution patterns were similar to those of the SAR, but much smoother. The maximum temperature elevations in the brain of 4- and 8-week-old rat models were 8.1°C and 10.8°C. The maximum temperature elevation in the 8-week-old rat model was 10.9°C, around the throat, similar to that observed in the brain.

3.3. Temperature elevation in live rats vs. numerical rat model

The temperature elevation computed using the rat model was compared with the measurement in live rats in order to validate the computational model (Fig. 5). In the parietal cortex, the time course of the computed temperature in the 4-week-old model was similar to the measured values. In addition, the time courses of the three temperatures measured fitted the values computed for each area.

However, in the 8-week-old model, only the maximum change in the computed temperature had a similar time course to the measured values. Measured temperatures were 1-2^{o}C higher than the temperature computed at the reference point at the end of MW exposure.

Rectum temperature elevated linearly during exposure. The computed temperature was 40% higher than the measured value in 4-week-old rats and 10% in 8-week-old animals.

3.4. Blood flow elevation in live rats vs numerical rat model

The blood flow variation computed using the rat model was compared with measurements in live rats (n=3 for each age) in order to validate the computational model (Fig. 6). The measured

blood flow varied widely, due to variations in vasomotion or arterial pressure. The median blood flow was comparable with the computed values. In 4-week-old rats, the time course of the blood flow in the model was quite similar to the measured values. The results were similar for 8-week-old rats, except that the measured blood flow elevated almost linearly.

3.5. Evaluation of the intensity-dependence of brain temperature elevations

Computed and measured temperature elevations in the brain were compared in order to evaluate the effectiveness of the computational model at different power input levels. As shown in Fig. 7, a good agreement was observed for 4-week-old rats, but not for 8-week-old rats at 150 or 300 W/kg.

4. Discussion

There are few computational models for simulating temperature variations and blood flow rates in the brain under intense local exposure. In the present study, we modeled these parameters for rats and validated the model by comparing our data with measurements in live rats.

4.1. Experimental conditions

Specific experimental conditions were set up in this in vivo study to focus on physiological changes caused by local MW exposure of the rat brain. First, the duration of the measurement, including the MW exposure, was determined to allow for the detection of changes in physiological parameters, and limited to 18 min under anesthesia. To assess the reversibility of parameter changes, we used three periods of 6 min each: pre-measurement, MW exposure, and post-exposure.

Second, temperature stabilization in each part of the body was achieved under sham-exposed conditions: the set temperatures of the heating pad (42^{o}C) and room (23^{o}C) were found to be optimal for this study and the mean temperature elevation above the initial rectal temperature was <0.1^{o}C over the 6-min period of sham exposure. Therefore, the temperature stabilization enabled us to measure a small temperature change due to MW exposure.

Third, reproducible changes in local cerebral blood flow were observed at the BASAR levels used in this study. Observable thermophysiological responses may not be detected at local exposure levels within the exposure limit range (ICNIRP 1998, IEEE 2005). Thus, very intense local exposure was needed to induce a response. The BASAR levels were based on a pilot study with a wide range of exposure intensity (0–300 W/kg BASAR). The exposure intensities at which irreversible changes were observed in local cerebral blood flow were eliminated from this study to investigate a relationship between blood flow and local temperatures.

4.2. Relationship between SAR and temperature elevation

In living organs/tissues, the presence of heat diffusion and transfer via blood flow affects local temperature elevations caused by local MW exposure. It was, therefore, suggested that the distributions of SAR and temperature elevations during exposure differed. These differences in distribution patterns were observed in our computational models. Although the temperature elevation distributions were similar to those of SAR, the former were much smoother than the latter, possibly due to heat diffusion.

In addition, the largest temperature elevation was observed around the throat, whereas the SAR in that area was lower than in the parietal region. This was apparently due to the fact that the blood flow rate in the throat (skin and fat) was lower than in the brain (See Table 1). In our previous experiment using rabbits, blood flow rate was the dominant factor influencing MW-induced temperature elevations (Hirata et al 2006).These previous findings concerning the role of heat diffusion and transfer were confirmed by this rat model.

4.3. Brain temperature elevation

Our models, allowing for the thermoregulatory response of cerebral blood flow (Eq. (9)), gave estimates of brain temperature elevations in good agreement with measured data, particularly at all SAR levels in the 4-week-old rat model. Under local exposure conditions, the estimation of temperature and blood flow is known to be strongly dependent on the computation location. Indeed, variations were observed in the computed time course of these parameters within the defined area of the parietal region. However, the variations in computed data were very similar to those in the measured values. Therefore, our findings suggest that the thermoregulatory response observed in the live rat brain was efficiently modeled, at least for 4-week-old rats.

However, in the case of 8-week-old rats, a good agreement was found only at the lowest intensity exposure. The computed brain temperature elevations tended to be smaller than the measured values (Fig. 5b). One of the reasons for this discrepancy may be an elevation in air temperature between the figure-8 antenna and the rat’s head, as the difference increased with the BASAR or brain hyperthermia (Fig. 7(b)). Taking this elevation in air temperature into account should give a better agreement between measured and computed temperature elevations. However, inserting an additional probe in this small gap may result in additional uncertainty. The main purpose of this study was to investigate the variations in blood flow rate due to localized exposure. Thus, further investigation into the role of air temperature in the gap will be included in the next study.

4.4. Rectal temperature elevation

The rectal temperature computed in both the model and the measured data elevated linearly (Fig.

5). However, the computed temperatures were 40% higher than the measured values for 4-week-old rats and 10% for 8-week-old animals.

One reason for these small differences may be an adjustment in the basal metabolic rate due to anesthesia. In the present study, the temperature change was measured in anesthetized rats. Anesthesia is known to influence the basal metabolism in rodents and the depth of anesthesia depends on the time after administration (Mishra 2002). Therefore, rectal temperature was regulated using a heating pad to offset the reduction in basal metabolism under anesthesia. However, the temperature change was not totally simulated in this model where the metabolic rate was fixed. It would be useful to reflect the dynamic change in basal metabolism in a future version of the model.

Another reason for the difference between measured and computed temperatures may be the difference in body weights between the voxel models and live rats. In the present study, only one numerical model consisting of a limited number of tissues was used for computation. It did not allow for variations in body weight at each age. In contrast, the standard deviations in body weights were 6% and 8% for the 4- and 8-week-old rats, respectively. Therefore, including weight variation factors should improve the accuracy of the rectal temperature computations.

4.5. Age-dependence in the thermoregulatory response model

In the present study, 4- and 8-week-old rats were used as juveniles and young adults, respectively, to investigate the age-dependence of thermophysiology. F_{RB} was not age-dependent, while F_{BB} was 40% smaller for 4-week-old than 8-week-old rats. However, it is noted that the contribution of F_{BB} to brain blood flow was much smaller than that of F_{RB}. The large contribution of F_{RB} was confirmed as shown in Fig. 7. We have so far focused on two age groups to evaluate the age-dependence of physiological change in the brain (Kukley et al 2001, Kuribayashi et al 2005). However, further studies using neonatal or aged rat are required to investigate whether the model developed here is valid for any age, since the lifespan of rat is about 24 months.

4.6. Extrapolation to human

The model developed here will help interpreting the physiological effects caused by local MW exposure and perform health risk assessment. However, there are still several issues pending, such as the extrapolation of the present model to the human thermophysiological. In this study, the effects of local MW exposure was assessed for less than 2 g of rat brain tissue while the basic restriction value for local exposure to MW in the ICNIRP guidelines is 2 W/kg (general public exposure) or 10 W/kg (occupational exposure) over 10 g of human brain tissue. Distribution of SAR and heat conduction during local MW exposure varies between rats and humans because of differences in body size and shape. However, the thermophysiological

relationship between local blood flow regulation and local temperature changes, which was found in the rat brain, might be similar in small regions of the human cortex.

5. Conclusions

In the present study, an electromagnetic-thermal computational code with an active blood flow model was developed to simulate electromagnetic power absorption and the resulting temperature elevations due to localized 1.457-GHz exposure of the rat brains. This modeling was motivated by the research need expressed by WHO. The computational model was validated by comparing its outcomes with data measured in 4- and 8-week-old rats. Despite some limitations in modeling active blood flow: i) administration of anesthetics was needed to measure blood flow rate and temperature in the brain and ii) temperature was only measured at the brain surface, due to the lack of space for inserting additional probes, the temperature elevations estimated by the model were in good agreement with measured data, especially for 4-week-old rats. Furthermore, the blood flow rate was found to depend on both rectal and brain temperature elevations. There were no obvious differences in the model between 4- and 8-week-old rats, under the exposure conditions used, though further validation of computational modeling (Neufeld et al 2009, Bakker et al 2010) and measurements may be needed.

The computational code developed here will be helpful in defining experimental conditions for further investigation of MW-induced thermophysiological changes. In addition, the model may be used in therapeutic application of hyperthermia and thermal ablation (Wust et al 2002, Franckena et al 2010, Fuentus et al 2011).

Appendix

A. Determination of Heating Pat

In the present study, a heating pad (42°C) was used to avoid a reduction in basal metabolism under anesthesia. Pad temperature was designed to maintain a constant rectal temperature in sham-exposed animals to compensate for the reduced basal metabolic rate induced by anesthesia. The main purpose of this study was not to develop the thermal model over the entire rat body but to estimate temperature variations in the brain due to localized exposure. The blood flow rate in the parietal region was also measured. For these reasons, the reduction in basal metabolic rate due to anesthesia was assumed to be uniform over the body.

The heat balance in the rat during MW exposure is given by the following equation:

$$M + P_{RF} - P_{conv} + P_{pad} = E \tag{13}$$

where M is the rate at which thermal energy is produced through metabolic processes, P_{RF} the MW power absorbed in the body, P_{conv} the rate of heat exchange via convection, E the rate of

heat storage in the body, and P_{pad} the rate of heat transfer from the pad. R_{RF} and E were not included for sham-exposed rats. Specifically, M and P_{conv} are identical to the parameters listed in Tables 1 and 2. Thus, the basal metabolic rate and blood flow rate are reduced to satisfy the heat balance in the rat. P_{pad} is estimated using the following equation:

$$P_{pad} = P_{conv} - \alpha M \tag{14}$$

$$P_{pad} = h(T_b - T_{pad})S \tag{15}$$

where α is the reduction rate in the basal metabolic rate and S the contact area between the rat model and the heating pad. The S values were 42.23 mm^2 and 60.90 mm^2 for 4- and 8-week-old rats, respectively, so the equation was balanced by reducing the metabolic rate by 33% and 38%, respectively.

B. Validity of Equations Introduced in Our modeling

In order to confirm our computational modeling with respect to a conventional study, the brain and core temperature elevations were also computed in the following two cases: (i) the blood flow in the tissues is assumed to be constant which means that vasodilatation governed by Eq. (9) is neglected, and (ii) the blood temperature is assumed to be constant which means that Eqs. (4) and (5) can be ignored. As a computational example, the 8-week-old rat model was exposed at a BASAR of 300 W/kg. In the case (ii), the blood temperature was not computed and thus the temperature in the position corresponding to the rectum was plotted for reference. As shown in Fig. 8, the brain temperature computed by neglecting the vasodilatation in the brain was twice as large as the measured one. The brain temperature computed by neglecting blood temperature variation was somewhat lower than the measured temperature. As shown in the measurement, the brain temperature continued to elevate along with the blood temperature. In the same figure, the core temperature was marginally affected even when neglecting vasodilatation in the brain. In addition, the temperature elevation in the rectum was much smaller than the measured value.

The variation in temperature in inner tissues, except for the brain tissue, was assumed to be constant as mentioned in Sec 2.4, even though the blood flow in the inner tissue was not measured. The blood flow in the remaining tissue would be affected by vasodilatation in the brain. The ΔT and α coefficients in Eqs. (11)-(12) were changed in order to quantify the uncertainty caused by our simplification. The 8-week-old rat model exposed at BASAR of 300 W/kg was again considered. As shown in Fig. 9, the brain temperature was best fitted for the parameter values of ΔT=1 and α=1, corresponding to an absence of thermoregulatory response. As presented in the previous study (Hirata et al 2006b), the thermoregulatory response in the remaining part of the body may be weaken due to the effect of anesthesia. As shown in Fig. 9,

further fine tuning of ΔT and α may not affect the temperature and blood flow in the brain.

Acknowledgement

We thank Drs. Akira Ushiyama and Shogo Hirota for their technical support.

References

Aalto S, Haarala C, Bruck A, Sipila H, Hamalainen H and Rinne J O 2006 Mobile phone affects cerebral blood flow in humans *J Cereb Blood Flow Metab* **26** 885-90

Adair E R and Adams B W 1980 Microwaves modify thermoregulatory behavior in squirrel monkey Bioelectromagnet. l 1-20

Adair E R, Adams B W, Akel G M 1984 Minimal changes in hypothalamic temperature accompany microwave-induced alteration of thermoregulatory behavior Bioelectromagnet. 5 13–30

Adair E R and Black D R 2003 Thermoregulatory responses to RF energy absorption. Bioelectromagnet. Suppl. 6 S17-38

American Conference of Government Industrial Hygienists (ACGIH), 1996 Threshold limit values for chemical substances and physical agents and biological exposure indices," (Cincinnati OH).

Arima T, Watanabe H, Wake K, Masuda H, Watanabe S, Taki M, and Uno T 2011 Local exposure system for rats head using figure-8 loop antenna in 1500 MHz Band IEEE Trans. Biomed. Eng. 58, 2740-2747.

Bakker J F, Paulides M M, Christ A, Kuster N and G C van Rhoon, 2010 Assessment of induced SAR in children exposed to electromagnetic plane waves between 10 MHz and 5.6 GHz. Phys. Med. Biol. **55**: 3115-3130.

Bernardi P, Cavagnaro M, Pisa S, Piuzzi E 2003 Specific absorption rate and temperature elevation in a subject exposed in the far-field of radio-frequency sources operating in the 10-900-MHz range IEEE Trans Biomed Eng. 50 295-304

Christ, A., Gosselin, M.C., Christopoulou, M., Kühn, S., Kuster, N., 2010. Age-dependent tissue-specific exposure of cell phone users. Phys. Med. Biol. 55, 1767-83.

Cooper T E and Trezek G J 1971 Correlation of thermal properties of some human tissue with water content. Aerospace Med. 50 24-7

Crezee J and Lagendijk J 1990 Experimental verification of bioheat transfer theories: measurement of temperature profiles around large artificial vessels in perfused tissue *Phys. Med. Biol* **35** 905-23

D'Andrea J A, DeWitt J R, Gandhi O P, Stensaas S, Lords J L, Neilson H C 1986 Behavioral and physiological effects of chronic 2450-MHz microwave irradiation of the rat at 0.5 mW/cm2

Bioelectromagnet. 7 45-56

D'Andrea J A, Adair E R, de Lorge J O 2003 Behavioral and cognitive effects of microwave exposure Bioelectromagnet. Supp. 7 S39 – 62

de Gannes F P, Taxile M, Duleu S, Hurtier A, Haro E, Geffard M, Ruffie G, Billaudel B, Leveque P, Dufour P, Lagroye I and Veyret B 2009 A confirmation study of Russian and Ukrainian data on effects of 2450 MHz microwave exposure on immunological processes and teratology in rats *Radiat Res* **172** 617-24

Ebert S, Eom S J, Schuderer J, Spostel U, Tillmann T, Dasenbrock C, and Kuster N 2005 Response, thermal regulatory threshold of restrained RF-exposed mice at 905 MHz. Phys. Med. Biol. 50 5203-15

Follow B and Neil E (ed) 1971 Circulation, Oxford University Press (New York USA)

Foster K R and Adair E R 2004 Modeling thermal responses in human subjects following extended exposure to radiofrequency energy. Biomed. Eng. Online 3 article no. 4

Franckena M, Canter R, Termorshuizen F, van der Zee J., van Rhoon G 2010 Clinical implementation of hyperthermia treatment planning guided steering: a cross over trial to assess its current contribution to treatment quality *Int. J. Hyperthermia* 26 145-157.

Fuentes D, Waler C, Elliott A, Shetty A, Hazle J D, Stafford R J 2011 Magnetic resonance temperature imaging validation of a bioheat transfer model for laser-induced thermal therapy. *Int. J. Hyperthermia* 27 453-464.

Fujimoto M, Hirata A, Wang J, Fujiwara O, and Shiozawa T 2006 FDTD-derived correlation of maximum temperature increase and peak SAR in child and adult head models due to dipole antenna, *IEEE Trans Electromagnet Compat* 48 240-247

Gabriel C. 1996. Compilation of the dielectric properties of body tissues at RF and microwave frequencies. Final Tech Rep Occupational and Environmental Health Directorate. AL/OE-TR-1996-0037 (Brooks Air Force Base, TX: RFR Division).

Gordon R G, Roemer R B, Horvath S. M. 1976 A mathematical model of the human temperature regulatory system—transient cold exposure response IEEE Trans. Biomed. Eng., 23, 434–444

Hirata A, Fujiwara O, and Shiozawa T 2006a Correlation between peak spatial-average SAR and temperature increase due to antennas attached to human trunk IEEE Trans. Biomed. Eng. 53 1658-64

Hirata A, Watanabe S, Taki M, Kojima M, Hata I, Wake K, Sasaki K, and Shiozawa T 2006a Computational verification of anesthesia effect on temperature variation in rabbit eyes exposed to 2.45-GHz microwave energy. Bioelectromagnetics 27: 602-612; 2006b.

Hirata A, Asano T, and Fujiwara O 2008 FDTD analysis of body-core temperature elevation in children and adults for whole-body exposure Phys Med Biol, 53, 5223-38

Hirata A, Sugiyama H, and Fujiwara O 2009a Estimation of core temperature elevation in humans and animals for whole-body averaged SAR Prog. Electromagnet. Res. 99 221-37

Hirata A and Fujiwara O 2009b Modeling time variation of blood temperature in a bioheat equation and its application to temperature analysis due to RF exposure Phys. Med. Biol. 54 N189-96

Hirata A, Kojima M, Kawai H, Yamashiro Y, Watanabe S, Sasaki H, and Fujiwara O 2010 Acute Dosimetry and estimation of threshold inducing behavioral signs of thermal stress in rabbits at 2.45-GHz microwave exposure IEEE Trans Biomed Eng 57 1234-42

Huber R, Treyer V, Schuderer J, Berthold T, Buck A, Kuster N, Landolt H P and Achermann P 2005 Exposure to pulse-modulated radio frequency electromagnetic fields affects regional cerebral blood flow *Eur J Neurosci* **21** 1000-6

Hoque M and Gandhi O P 1988 Temperature distribution in the human leg for VLF-VHF exposure at the ANSI recommended safety levels IEEE Trans Biomed Eng 35 442-49.

IEEE C95.1 2006 IEEE standard for safety levels with respect to human exposure to radio frequency electromagnetic fields, 3 kHz to 300 GHz. New York: IEEE

International Commission on Non-Ionizing Radiation Protection (ICNIRP) 1998 Guidelines for limiting exposure to time-varying electric, magnetic, and electromagnetic fields (up to 300 GHz). Health Phys. 74 494-522

International Commission on Non-Ionizing Radiation Protection (ICNIRP) 2009 Exposure to high frequency electromagnetic fields, biological effects and health consequences (100 kHz-300GHz) Available: http://www.icnirp.de/documents/RFReview.pdf

International Commission on Radiological Protection (ICRP) 1975 Report of the Task Group on Reference Man 23 Pergamon Press: Oxford; 1975.

Kukley M, Barden J A, Steinhauser C and Jabs R 2001 Distribution of P2X receptors on astrocytes in juvenile rat hippocampus *Glia* **36** 11-21

Kuribayashi M, Wang J, Fujiwara O, Doi Y, Nabae K, Tamano S, Ogiso T, Asamoto M and Shirai T 2005 Lack of effects of 1439 MHz electromagnetic near field exposure on the blood-brain barrier in immature and young rats *Bioelectromagnetics* **26** 578-88

Lee H B and Blaufox M D 1985 Blood volume in the rat J. Nucl. Med. 25 72-7

Mishra L D 2002 Cerebral blood flow and anesthesia: a review Indian J Anaesth 20 87-95

Marai I F M, Habeeb A A M, and Gad A E 2002 Rabbits' productive, reproductive and physiological performance traits as affected by heat stress: a review. Livestock Prod. Sci. 78 71-90.

Masuda H, Ushiyama A, Hirota S, Wake K, Watanabe S, Yamanaka Y, Taki M and Ohkubo C 2007 Effects of subchronic exposure to a 1439 MHz electromagnetic field on the microcirculatory parameters in rat brain *In. Vivo.* **21.** 563-70

Masuda H, Ushiyama A, Takahashi M, Wang J, Fujiwara O, Hikage T, Nojima T, Fujita K, Kudo M and Ohkubo C 2009 Effects of 915 MHz electromagnetic-field radiation in TEM cell on the blood-brain barrier and neurons in the rat brain *Radiat Res* **172** 66-73

Masuda H, Hirata A, Kawai H, Watanabe S, Arima T, de Gannes F P, Lagroye I, and Veyret B 2011 Local exposure of the rat cortex to radiofrequency electromagnetic fields increases local cerebral blood flow along with temperature J. Appl. Physiol. 110 142-8.

McQuade J M, Merritt J H, Miller S A, Scholin T, Cook M C, Salazar A, Rahimi O B, Murphy M R and Mason P A 2009 Radiofrequency-radiation exposure does not induce detectable leakage of albumin across the blood-brain barrier *Radiat Res* **171** 615-21

Michaelson S M 1983 Biological effects and health hazard of RF and MW energy; fundamentals and overall phenomenology. In: Biological effects and dosimetry of nonionizing radiation (M. Grandolfo, S. M. Michaelson, and A. Rindi, eds.) New York, Plenum Press, 337-57.

Mizuno Y, Moriguchi Y, Hikage T, Terao Y, Ohnishi T, Nojima T and Ugawa Y 2009 Effects of W-CDMA 1950 MHz EMF emitted by mobile phones on regional cerebral blood flow in humans *Bioelectromagnetics* **30** 536-44

Neufeld E, Kuhn S, Szekely G, and Kuster N 2009 Measurement, simulation and uncertainty assessment of implant heating during MRI Phys Med Biol **41**51-71.

Peyman A, Rezazadeh A, and Gabriel C 2001 Changes in the dielectric properties of rat tissue as a function of age at microwave frequencies **46** 1617-

Peyman A 2011 Dielectric properties of tissues; variation with age and their relevance in exposure of children to electromagnetic fields; state of knowledge (in press)

Pennes H H 1948 Analysis of tissue and arterial blood temperatures in resting forearm J. Appl. Physiol. 1: 93-122

Salford L G, Brun A E, Eberhardt J L, Malmgren L and Persson B R 2003 Nerve cell damage in mammalian brain after exposure to microwaves from GSM mobile phones *Environ Health Perspect* **111** 881-3

Stern S, Margolin L, Weiss B, Lu S, Michaelson S M 1979 Microwaves: effects on thermoregulatory behavior in rats. Science 206 198-201

Taflove A and Hagness S. Computational Electrodynamics: The Finite-Difference Time-Domain Method: 2nd Ed. Norwood. MA: Artech House, 1995.

Tuma R F, Irion G L, Vasthare U S, Heinel L A 1985 Age-related changes in regional blood flow in the rat, Am J Physiol 249 H485-91

World Health Organization (WHO), RF research agenda, 2006. Available: http://www.who.int/peh-emf/research/rf_research_agenda_2006.pdf

Wust P, Hildebrandt G, Sreenivasa G, Rau B, Gellermann J, Riess H, Felix R, Schlag P M. 2002

Hyperthermia in combined treatment of cancer *Lancet Oncol*. 3 487-97.

FIGURE AND TABLE CAPTIONS

Table 1. Dielectric properties of rats. The same constants were used for 4- and 8-week-old rats.

Table 2. Thermal conductivity K, specific heat C, blood perfusion rate B_0, and basal metabolism A_0 of tissues in anesthetized rats; (a) 4- and (b) 8-week-old rats.

Figure1. Schematic diagram of the rat exposure system. The figure-8 antenna was located above the rat's head. The heating pad was inserted under the rat body to compensate for the temperature decrease due to anesthesia.

Figure 2. Defined area for calculating the temperature elevation in the parietal region of (a) 4- and (b) 8-week-old rat models.

Figure 3. Distributions of voxel SAR (a) and temperature elevation (b) in the 4-week-old rat model. Brain averaged SAR: 167 W/kg. Exposure duration: six minutes.

Figure 4. Distributions of voxel SAR (a) and temperature elevation (b) in the 8-week-old rat. Brain averaged SAR: 300 W/kg. Exposure duration: six minutes.

Figure 5. Temperature elevations in the parietal region and rectum during MW exposure. The brain averaged SARs for 4- and 8-week-old rats were 167 W/kg and 300 W/kg, respectively. The temperature elevation in the parietal region was calculated at each voxel within the defined area. The minimum and maximum temperature elevations in the area are indicated as broken lines. A solid line shows the elevation at the reference point. Typical temperature changes measured in the parietal region and rectum of live rats (n=3 for each age) are plotted for comparison with computed values. (a) 4-week-old rat and (b) 8-week-old rat.

Figure 6. Blood flow increases in the parietal region during MW exposure. The brain averaged SARs for 4- and 8-week-old rats were 167 W/kg and 300 W/kg, respectively. The blood flow increase in the parietal region was calculated at each voxel within the defined area. The minimum and maximum increases in blood flow in the area are indicated as broken lines. A solid line shows the increase at the reference point. Typical blood flow changes measured in the parietal region of live rats (n=3 for each age) are plotted for comparison with computed values. (a) 4-week-old rat, (b) 8-week-old rat.

Figure 7. Temperature elevation in the parietal region at different BASARs. The solid line is the

computed temperature at the reference point. Median values of measured temperatures (n=6 for each intensity) are plotted for comparison with computed values. (a) 4-week-old rat and (b) 8-week-old rat.

Figure 8. Temperature elevations in the parietal region and rectum of 8-week-old rat during MW exposure at BASAR of 300 W/kg for different computational modeling; i) the blood perfusion rates of tissues and ii) the blood temperature are assumed to be constant over the body

Figure 9. Temperature elevations in the parietal region of 8-week-old rat during MW exposure at BASAR of 300 W/kg for different parameters characterizing the blood perfusion rate in the inner tissues.

Table 1

Tissue	Relative Permittivity	Conductivity [S/m]
Skin	33.5	0.94
Muscle	47.4	1.38
Fat	11.1	0.16
Bone	23.8	0.65
Brain	46.7	1.15
Eye	68.7	1.89

Table 2

(a)

Tissue	K [W/(m ^{o}C)]	C [J/(kg ^{o}C)]	B_0 [W/(m^3 ^{o}C)]	A_0 [W/m^3]
Skin	0.42	3600	17163	10008
Muscle	0.50	3800	562	2484
Fat	0.25	3000	9316	5432
Bone	0.37	3100	12317	10622
Brain	0.57	3800	18216	12936
Eye	0.58	4000	0	0
Blood	0.58	3900	-	-

(b)

Tissue	K [W/(m ^{o}C)]	C [J/(kg ^{o}C)]	B_0 [W/(m^3 ^{o}C)]	A_0 [W/m^3]
Skin	0.42	3600	11605	7486
Muscle	0.50	3800	380	1858
Fat	0.25	3000	6299	4063
Bone	0.37	3100	12317	7945
Brain	0.57	3800	16800	10837
Eye	0.58	4000	0	0
Blood	0.58	3900	-	-

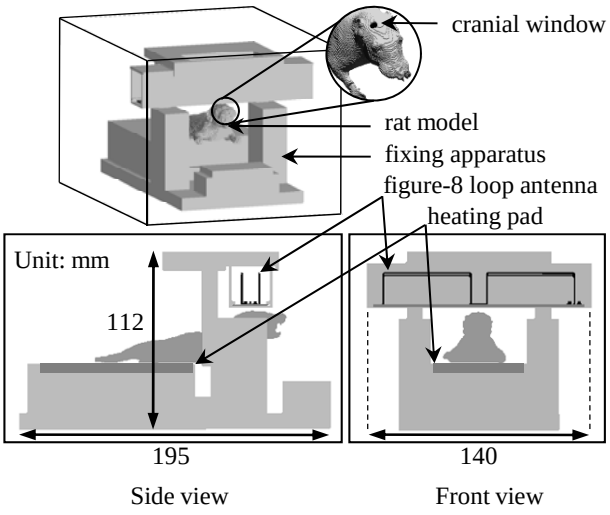

Figure 1

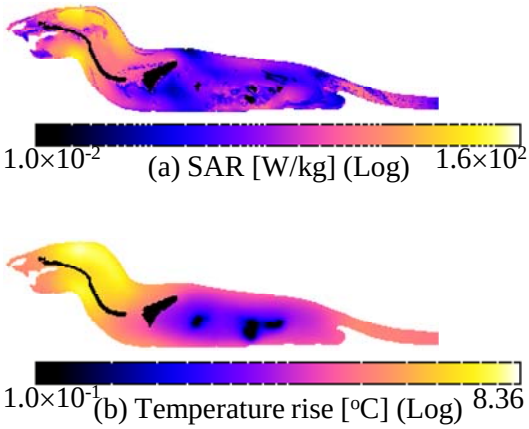

Figure 2

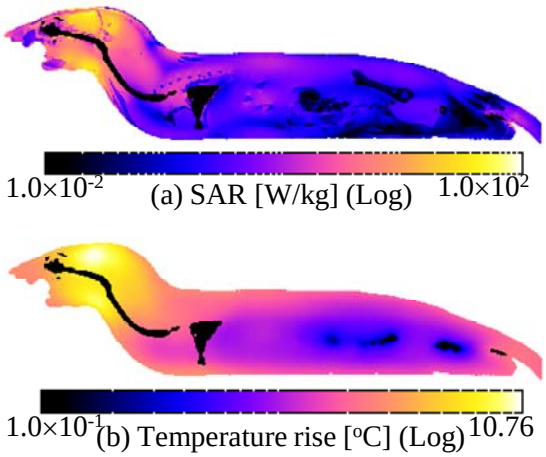

Figure 3

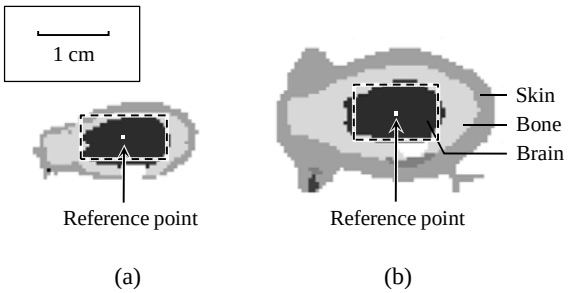

Figure 4

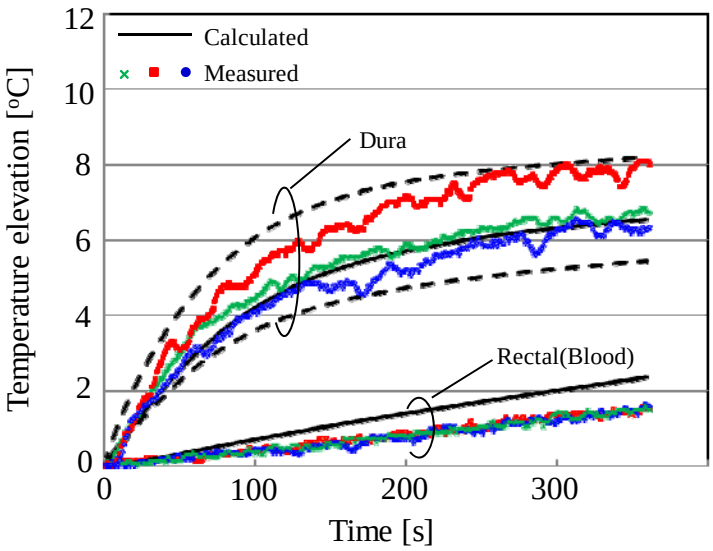
Calculated
Measured
Dura
Rectal(Blood)
Temperature elevation [°C]
Time [s]
0
2
4
6
8
10
12
0
100
200
300

(a)

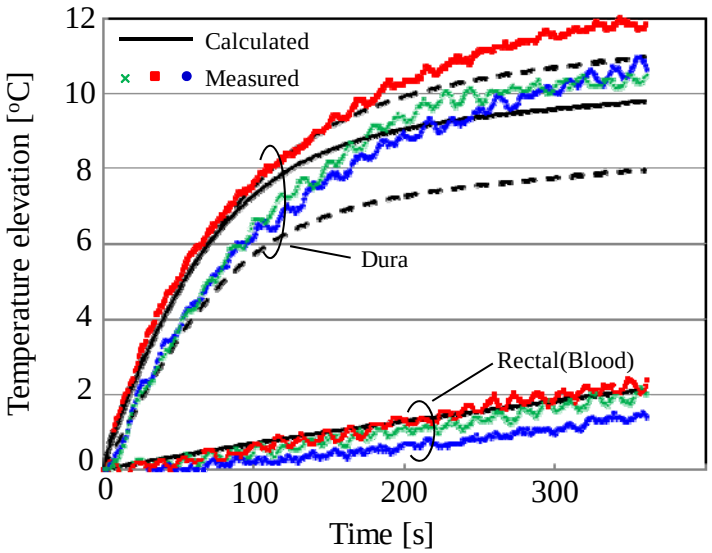
Calculated
Measured
Dura
Rectal(Blood)
Temperature elevation [°C]
Time [s]
0
2
4
6
8
10
12
0
100
200
300

(b)

Figure 5

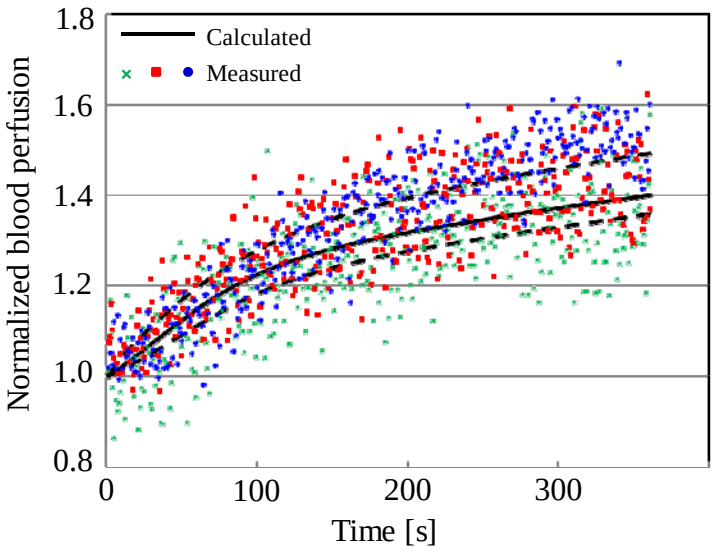
Calculated
Measured
Normalized blood perfusion
1.8
1.6
1.4
1.2
1.0
0.8
0
100
200
300
Time [s]

(a)

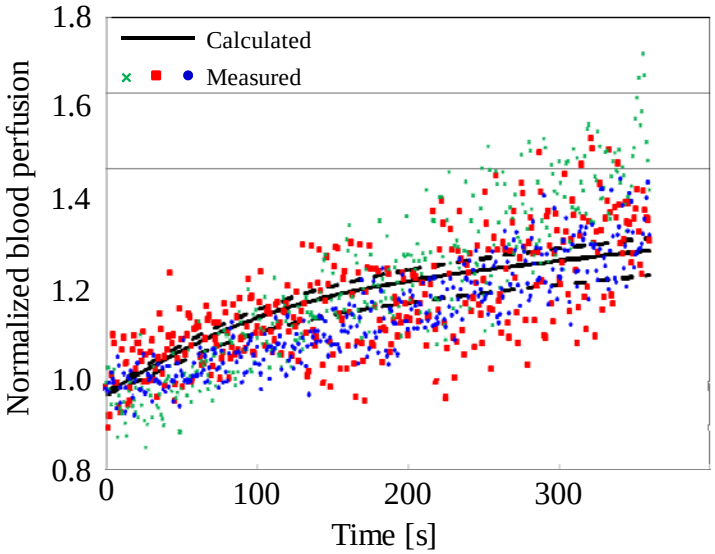
Calculated
Measured
Normalized blood perfusion
1.8
1.6
1.4
1.2
1.0
0.8
0
100
200
300
Time [s]

(b)

Figure 6

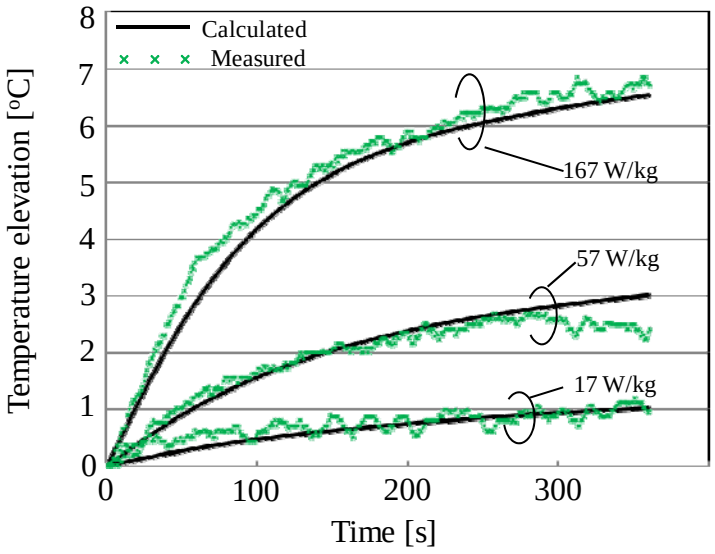
Calculated
Measured
Temperature elevation [°C]
Time [s]
167 W/kg
57 W/kg
17 W/kg
0
1
2
3
4
5
6
7
8
0
100
200
300

(a)

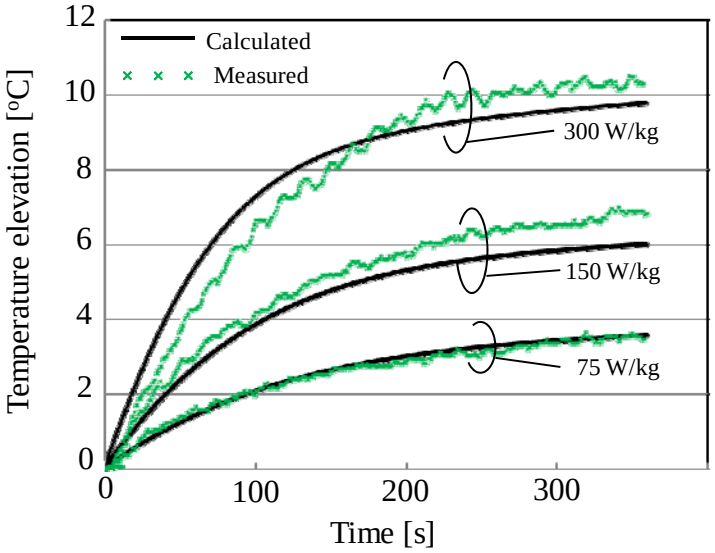
Calculated
Measured
Temperature elevation [°C]
Time [s]
300 W/kg
150 W/kg
75 W/kg
0
2
4
6
8
10
12
0
100
200
300

(b)

Figure 7

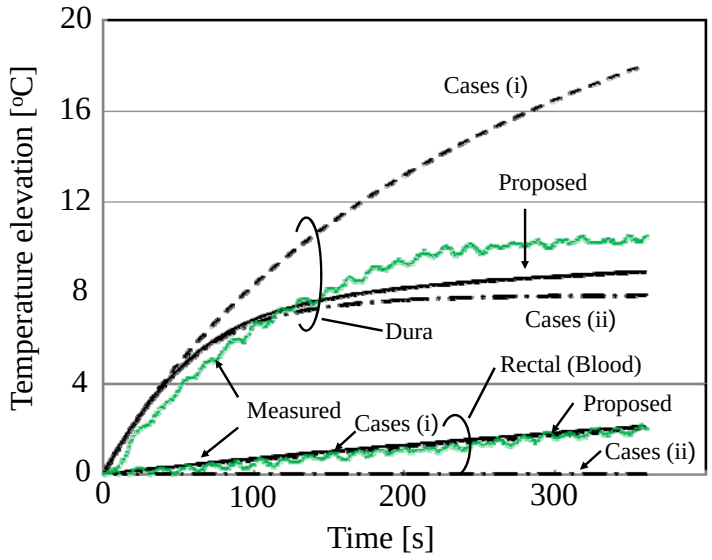
Temperature elevation [°C]
20
16
12
8
4
0
0
100
200
300
Time [s]
Cases (i)
Proposed
Cases (ii)
Dura
Rectal (Blood)
Measured
Cases (i)
Proposed
Cases (ii)

Fig. 8

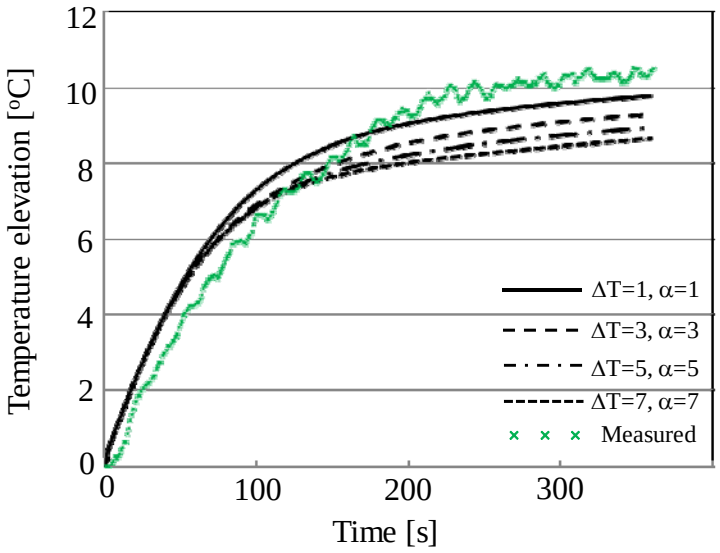
Temperature elevation [°C]
12
10
8
6
4
2
0
0
100
200
300
Time [s]
ΔT=1, α=1
ΔT=3, α=3
ΔT=5, α=5
ΔT=7, α=7
Measured

Fig. 9